An Inner Pore Residue (Asn406) in the $Na_v1.5$ Channel Controls Slow Inactivation and Enhances Mibefradil Block to T-Type Ca^{2+} Channel Levels

Megan M. McNulty, John W. Kyle, Gregory M. Lipkind, and Dorothy A. Hanck

Departments of Medicine (M.M.M., J.W.K, D.A.H.) and Biochemistry and Molecular Biology (G.M.L.), University of Chicago, Chicago, Illinois

ABSTRACT

Mibefradil is a tetralol derivative once marketed to treat hypertension. Its primary target is the T-type Ca^{2+} channel (IC_{50}, ~0.1–0.2 μM), but it also blocks Na^+, K^+, Cl^-, and other Ca^{2+} channels at higher concentrations. We have recently reported state-dependent mibefradil block of Na^+ channels in which apparent affinity was enhanced when channels were recruited to slow-inactivated conformations. The structural determinants controlling mibefradil block have not been identified, although evidence suggests involvement of regions near or within the inner pore. We tested whether mibefradil interacts with the local anesthetic (LA) binding site, which includes residues in the S6 segments of domains (D) I, III, and IV. Mutagenesis of DIII S6 and DIVS6 did not reveal critical binding determinants. Substitution of Asn406 in DI S6 of cardiac $Na_v1.5$, however, altered affinity in a manner dependent on the identity of the substituting residue. Replacing Asn406 with a phenylalanine or a cysteine increased affinity by 4- and 7-fold, respectively, thus conferring T-type Ca^{2+} channel-like mibefradil sensitivity to the Na^+ channel. A series of other substitutions that varied in size, charge, and hydrophobicity had minimal effects on mibefradil block, but all mutations dramatically altered the magnitude and voltage-dependence of slow inactivation, consistent with data in other isoforms. Channels did not slow-inactivate, however, at the voltages used to assay mibefradil block, supporting the idea that Asn406 lies within or near the mibefradil binding site.

Mibefradil (Ro 40-5967), a novel Ca^{2+} channel antagonist once marketed to treat hypertension and angina, cross-reacts with other ion channels. Although best known for its high-affinity blockade of T-type Ca^{2+} channels, mibefradil also blocks various classes of K^+ (Chouabe et al., 1998; Perchenet and Clement-Chomienne, 2000), Cl^- (Nilius et al., 1997), and Na^+ (Eller et al., 2000; Guatimosim et al., 2001; McNulty and Hanck, 2004) channels. This cross-reactivity not only raises the possibility that its in vivo cardiovascular effects resulted from interaction with multiple targets but also suggests that mibefradil interacts with common structural motifs across channels. Elucidating the details underlying channel-drug interactions responsible for mibefradil block could provide valuable structural and kinetic insights into mibefradil's targets and potentially facilitate the design of future antihypertensive agents.

Although the structural channel determinants controlling mibefradil affinity have not been molecularly identified in any of its targets, available evidence, including our recent report describing mibefradil block of Na^+ channels (McNulty and Hanck, 2004) and drug competition assays in Ca^{2+} channels (Rutledge and Triggle, 1995), suggests that mibefradil interacts with the channel in or near the inner pore. Na^+ channels share a predicted membrane topology with Ca^{2+} channels consisting of a single pore-forming polypeptide (α subunit) made up of four homologous domains (DI–DIV), each domain with six transmembrane spanning segments (S1–S6). The channel pore is thought to be lined with the 6th transmembrane segment (S6) from each domain (Fozzard and Hanck, 1996; Catterall, 2000), and these segments contribute to the formation of multiple drug binding sites in both classes of channels. Therefore, it is quite possible that these diverse classes of channels share an architecture that facilitates mibefradil binding, and such information in one channel is likely to be applicable in other targets.

We have described the characteristics of mibefradil block of

cardiac Na$^+$ channels (Na$_v$1.5) stably expressed in human embryonic kidney 293 cells (McNulty and Hanck, 2004); mibefradil exhibited greater block when channels were recruited to slow-inactivated conformations relative to closed and fast-inactivated states. This characteristic of block is similar to other Na$^+$ channel blockers, such as the local anesthetic (LA) class. We sought to determine, therefore, whether residues important for LA block of Na$^+$ channels also control mibefradil block. An assay of mutations at positions implicated in controlling lidocaine-like drug affinity (for review, see Catterall, 2002), however, identified only one site of importance for mibefradil block, an asparagine located near the intracellular side of DI S6 (located at position 434 in skeletal muscle Na$_v$1.4, 418 in brain Na$_v$1.2, and 406 in cardiac Na$_v$1.5) that has been shown to be important for determining the affinity of various compounds, including local anesthetics and batrachotoxin (Wang and Wang, 1998; Wang et al., 1998; Nau et al., 1999; Yarov-Yarovoy et al., 2002; Kondratiev and Tomaselli, 2003). Mutations at this position have also been shown to exhibit significant effects on channel gating, with particularly dramatic alterations on the entry into slow-inactivated states (Wang and Wang, 1997; Nau et al., 1999; Yarov-Yarovoy et al., 2002; Kondratiev and Tomaselli, 2003) dependent on the identity of the substituting residue. Most of these studies assayed gating effects in the skeletal muscle (Na$_v$1.4) or brain (Na$_v$1.2) isoforms, raising the question of whether this position controls gating in an isoform-dependent manner, which we addressed by performing the same mutations in the cardiac Na$_v$1.5 background. Furthermore, in light of mibefradil's interaction with slow-inactivated channels (McNulty and Hanck, 2004), and the role of this position in drug block and slow inactivation gating, we tested whether this asparagine could control mibefradil affinity either independently or in conjunction with its effects on slow inactivation.

Materials and Methods

Heterologous Expression. The cDNA for the human heart voltage-gated Na$^+$ channel, Na$_v$1.5 (hH1a), was kindly provided by H. Hartmann (University of Maryland) and A. Brown (Chantest Inc., Cleveland, OH) (Hartmann et al., 1994). Na$_v$1.4 (skeletal muscle, μ1) cDNA was originally from Gail Mandel (Stony Brook University, Stony Brook, NY). Site-directed mutagenesis at Asn406 was performed using the QuikChange site-directed mutagenesis kit (Stratagene, La Jolla, CA) according to the manufacturer's protocols. The cDNAs were subcloned into the mammalian expression vectors pcDNA5/FRT and transfected into human embryonic kidney 293/FLP (Invitrogen, Carlsbad, CA) cells using the calcium-phosphate or Lipofectamine Plus (Invitrogen) transfection methods and selected with 100 μg/ml Hygromycin B or HygroGold (Sigma, St. Louis, MO). In comparisons, WT refers to Na$_v$1.5 or Na$_v$1.5 C373Y as appropriate for the background in which the mutations were made; these are indicated in the figure legends. Cells were maintained in Dulbecco's modified Eagle's medium (Invitrogen) supplemented with 10% fetal bovine serum, 50 units/ml penicillin, 50 μg/ml streptomycin, and selection antibiotic. Whole-cell voltage clamp was performed on trypsinized cells (0.25% Trypsin-EDTA; Invitrogen) 3 to 6 days after plating.

Solutions and Chemicals. Pipette solution contained 100 mM CsF, 40 mM CsCl, 5 mM NaCl, 10 mM HEPES, and 10 mM EGTA, pH adjusted to 7.4 with CsOH. The bath solution contained 10 mM NaCl, 130 mM CsCl, 10 mM HEPES, and 2 mM CaCl$_2$, pH 7.4 with CsOH. For some cell lines, higher concentrations of Na$^+$ were used ([70 mM]$_o$; [40 mM]$_i$). It should be noted that differences in extracellular Na$^+$ concentration may result in quantitative differences in the magnitude of slow inactivation as higher concentrations slow the entry into and speed the recovery from slow-inactivated states (Townsend and Horn, 1997). Under our conditions, however, the fraction of channels slow-inactivated were minimally affected by the increase from 10 to 70 mM [Na]$_o$; therefore, the difference in extracellular Na$^+$ alone cannot account for the dramatic changes in slow inactivation exerted by the mutations. Mibefradil (Sigma) was freshly diluted in bath solution to the desired concentration (0.1–50 μM) from a stock solution (1 or 10 mM in distilled water stored in the dark at approximately 8°C).

Electrophysiological Recordings and Analysis. All recordings were made at room temperature using the whole-cell voltage-clamp configuration. Patch pipettes were pulled from thin-walled borosilicate (World Precision Instruments, Inc., Sarasota, FL), Garner 8250 (Garner Glass, Claremont, CA), or Fisherbrand microhematocrit (Fisher Scientific Co., Pittsburgh, PA) glass capillaries using the Flaming/Brown micropipette puller P97 (Sutter Instruments, Novato, CA) and had resistances of 0.6 to 1.2 MΩ when filled with pipette solution. All recordings were made using an Axopatch 200 or 200B feedback amplifier (Axon Instruments, Union City, CA) with a National Instruments PXI-6052E digital-to-analog converter and LabView 7.0 data acquisition software (National Instruments Corporation, Austin, TX) or with a Digidata 1320A or 1321A digital-to-analog converter with pClamp 8 data acquistion software (Axon Instruments). Data were filtered at 10 kHz using an eight-pole, low-pass Bessel filter and sampled at 20 kHz.

Drug was applied using either a single chamber bath in which solutions were exchanged using a Lee 3-way latching subminiature solenoid valve (The Lee Company, Westbrook, CT) switch system or a multichamber bath in which cells sealed to the patch pipette were lifted and moved from chamber to chamber to measure currents in the absence and presence of drug. Details of voltage protocols to assay drug effects are given under *Results*.

Data were analyzed using locally written programs in MatLab 7.0 (The Mathworks, Inc., Natick, MA). Ionic current data were capacity-corrected using 8 to 16 subthreshold responses (voltage steps of 10 or 20 mV) and leak-subtracted, based on linear leak resistance calculated from currents between -80 mV and the holding potential or linear interpolation between the current at the holding potential and 0 mV. Only cells with a leak resistance of approximately 500 MΩ or greater were included in the pooled data. Curve fitting and statistical analysis (Student's t test) were performed using MatLab (The Mathworks, Inc., Natick, MA) and Origin software (OriginLab Corp, Northampton, MA). A p value of <0.05 was considered significant. Data are depicted as means $\pm$ S.E.M.

Results

The structural determinants that contribute to mibefradil block have not been identified in any of its channel targets, although multiple lines of evidence, including our recently published data in Na$^+$ channels (McNulty and Hanck, 2004), suggest that mibefradil interacts with the inner pore via an access path from the intracellular side of the channel. The Na$^+$ channel blocking local anesthetic drugs (LAs), such as lidocaine, also seem to bind in the inner pore, and specifically a defined set of residues in the S6 segments of DI (Asn406, according the Na$_v$1.5 numbering), DIII (Leu1461), and DIV (Phe1759 and Tyr1766) (Fig. 1A, $*$) have been implicated in LA block (Catterall, 2002). We screened these residues for involvement in mibefradil binding by assaying fractional block at a drug concentration near the WT IC$_{50}$ to predict an apparent affinity. In these studies, therefore, apparent affinity refers to mibefradil concentrations that inhibited Na$^+$

currents by 50% as measured electrophysiologically. To avoid confusion arising from gating differences across channel mutants, drug was applied while cells were held at a negative potential at which channels were fully available (−130 or −140 mV for WT; −150 or −160 mV for mutants) and depolarized infrequently, once every 5 s (0.2 Hz). Mutations were performed in the cardiac muscle $Na_v1.5$ channel and/or the skeletal muscle $Na_v1.4$ cDNAs. Both channels have a similar affinity for mibefradil under these conditions (McNulty and Hanck, 2004). Alanine or cysteine substitutions of a DIII S6 residue (Leu1461) and two DIV S6 residues (Phe1759, Tyr1766) thought to be the most critical in controlling LA affinity produced less than a 3-fold change in the apparent affinity for mibefradil compared with WT (Fig. 1B). Extending the analysis to other nearby S6 residues in DII, DIII, and DIV (Leu931 and Phe934 in DII; Ile1465 in DIII; Val1763 and Ile1769 in DIV) also failed to reveal critical binding determinants (Fig. 1B). A residue in DI S6 (Asn406), also thought to be involved in LA block, however, increased affinity dramatically when mutated to a cysteine. Concentration-response data confirmed the initial screening results demonstrating an IC_{50} in N406C channels that was more than 7-fold lower than WT (0.4 μM versus 2.9 μM) (Fig. 2A). The cysteine substitution thus conferred a T-type Ca^{2+} channel-like affinity [140–200 nM (Martin et al., 2000)] to the cardiac Na^+ channel. Not only is Asn406 well positioned to interact with mibefradil directly or to allosterically influence its binding, but as a residue that is highly conserved across both Na^+ and Ca^{2+} channels, it may form part of a common structural motif that allows mibefradil to interact with multiple targets.

The asparagine at this position in DI S6 is a common drug block determinant across Na^+ channel isoforms, having been previously implicated in both local anesthetic and batrachotoxin block (Wang and Wang, 1998; Nau et al., 1999; Yarov-Yarovoy et al., 2002). In skeletal muscle channels, this mutation ($Na_v1.4$ N434C) enhanced both rested-state and use-dependent block of the local anesthetics bupivacaine (Nau et al., 1999) and lidocaine (Kondratiev and Tomaselli, 2003). These higher apparent affinities were attributed, at least in part, to enhanced channel inactivation, and more detailed analyses of mutations at this position revealed an increase specifically in slow inactivation (Wang and Wang, 1997; Nau et al., 1999; Kondratiev and Tomaselli, 2003). Our recent report detailing mibefradil's state-dependence in Na^+ channels revealed relatively high affinity for channels recruited to one or more slow-inactivated conformations (McNulty and Hanck, 2004). We therefore sought to determine whether there was a correlative change in mibefradil affinity in channels exhibiting enhanced slow inactivation as a result of the Asn-to-Cys mutation at position 406 in the cardiac isoform ($Na_v1.5$). Slow inactivation was tested using a two-pulse protocol in which cells were conditioned for 50 s at different potentials and hyperpolarized briefly (40 ms) to recover fast-inactivated channels before testing for availability. In $Na_v1.5$, a 50-s conditioning prepulse is $6 \times \tau$ for development of slow inactivation at −10 mV (McNulty and Hanck, 2004). Consistent with the enhancement of slow inactivation observed in the $Na_v1.4$ background (Nau et al., 1999), the Cys substitution also enhanced slow inactivation in the cardiac $Na_v1.5$ channel (Fig. 2B; Table 2), indicating that the role of
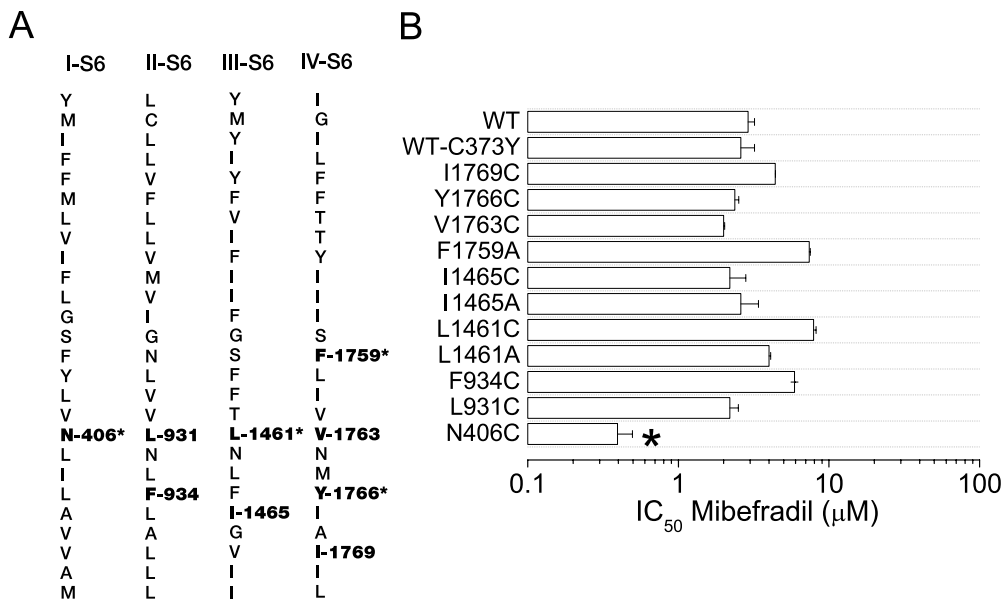

Fig. 1. Mibefradil block of channels with mutations in pore-lining residues, including those implicated in LA block. A, proposed alignment of the S6 segment from each domain highlighting the residues identified in controlling the apparent affinity of local anesthetics (marked in bold and with an asterisk) and additional S6 residues (in bold) tested for mibefradil block. B, mibefradil IC_{50} values for each of the mutations tested. All mutations were made in the cardiac muscle $Na_v1.5$ C373Y channel, except for N406C, which was made in $Na_v1.5$; one position (Y1766C) was also studied in the skeletal muscle background (at Y1586C), which exhibits a cardiac channel-like affinity for mibefradil (McNulty and Hanck, 2004); thus, those data are pooled. Drug was applied while cells were held at negative potentials (−130 or −140 mV for WT; −150 or −160 mV for mutants) to ensure full channel availability and depolarized infrequently, once every 5 s (0.2Hz). Fractional block, assayed at one or more drug concentrations (1–10 μM) near the WT IC_{50} value we reported previously [2.9 μM (McNulty and Hanck, 2004)], was determined by normalizing the peak current (average of at least 10 sweeps) after the drug effect had reached steady state to the peak current measured in the absence of drug. The IC_{50} value was determined by fitting a single site binding curve (blocked fraction = [mibefradil]/(IC_{50} + [mibefradil])) to the data (n = 2–6 for each mutation). The IC_{50} values for N406C and WT C373Y were derived from data presented in Figs. 2 and 3, respectively, and compared with WT $Na_v1.5$ data taken from McNulty and Hanck (2004); ∗, $p < 0.05$. N406C was >7-fold more sensitive to mibefradil than WT. A Bonferroni t test was used to evaluate all other data at 5 μM. Only the L1461C dataset achieved statistical significance, but the effect was less than 3-fold.

this position in slow inactivation applies across Na$^+$ channel isoforms.

The increase in apparent mibefradil affinity with the Cys substitution might arise through a direct alteration in the drug binding site or indirectly through allosteric changes in the binding site and/or effects on channel gating. Even though the conditions under which we assayed mibefradil block were such as to heavily discourage occupancy in slow-inactivated states, the cysteine substitution could be enhancing affinity by increasing the propensity for channels to occupy slow-inactivated conformations, states known to exhibit

Fig. 2. Mibefradil block and slow inactivation of Na$_v$1.5 N406C channels. A, concentration-response data for mibefradil block of wild type Na$_v$1.5 channels [taken from our previously published work (McNulty and Hanck, 2004)] and Na$_v$1.5 N406C channels. Mibefradil was applied during low-frequency (0.2 Hz) depolarizations to -30 or -10 mV from holding potentials that ensured full channel availability (WT, -130 or -140 mV; N406C, -150 or -160 mV). Fractional block was determined as described in Fig. 1. Data were fit with single-site binding curves to obtain IC$_{50}$ values: WT, 2.9 ± 0.4 μM ($n = 5$–6 from McNulty and Hanck, 2004); N406C, 0.39 ± 0.1 μM, ($n = 2$–7 at each concentration). B, slow inactivation of N406C. Slow inactivation was measured with a two-pulse protocol (inset). Cells were conditioned at different potentials for 50 s, hyperpolarized to -160 mV for 40 ms to recover fast-inactivated channels, and depolarized to -10 mV to test for channel availability. Cells were held at -160 mV for at least 35 s in between sweeps to ensure complete recovery from inactivation. Currents measured during the test pulse were normalized to peak test currents elicited in the absence of inactivating prepulses recorded before and after the slow-inactivation protocols. A linear regression describing time-dependent decreases in test current was used in the normalization to correct for changes in peak current unrelated to channel inactivation. Slow inactivation parameters were estimated by fitting the averaged data plotted as a function of the conditioning prepulse to a Boltzmann distribution: Fraction Available = [S_2 + $(1 - S_2)/(1 + \exp^{[(V - V_{1/2})/dx]})$], where $V_{1/2}$ is the voltage half-point of slow inactivation, dx is the slope factor, and S_2 is the steady-state fraction of availability. Parameters from the fits are given in Table 2. WT, $n = 3$; N406C, $n = 7$ or 8 at each potential.

higher affinity for mibefradil. We would predict, therefore, that other mutations that affect the fraction of channels entering these states would affect the apparent affinity for mibefradil. We tested for this general phenomenon by comparing mibefradil block in the WT Na$_v$1.5 with a channel in which an outer pore residue (Cys373) was mutated to the Tyr. This change dramatically affects affinity of the channel for tetrodotoxin, increasing it almost 1000-fold (Satin et al., 1992). Therefore, it is often used in mutational studies as the background in which other mutations are introduced. The C373Y channel has kinetics largely similar to those of WT Na$_v$1.5 (Table 1) but it exhibits less slow inactivation than WT (Fig. 3A; Table 2). Only 47% of C373Y channels slow-inactivated with a 50-s pulse to -10 mV compared with 61% of WT channels. One might expect that if affinity at negative potentials were affected by the propensity of channels to enter slow-inactivated states (mass action), then mibefradil affinity would be lower. However, even though this mutant channel slow-inactivated less well, block by mibefradil was indistinguishable between the channels (Fig. 3B; IC$_{50}$ values: C373Y, 2.6 μM; WT, 2.9 μM).

It might be that the differences in slow inactivation between the C373Y and WT channels were too modest to reveal a link between the slow-inactivated conformation and mibefradil affinity or that the conformation of the C373Y channel differs from that achieved with mutations in the inner pore. We therefore turned our attention to other substitutions at Asn406. Nau et al. (1999) demonstrated that substitution of Asn with the positively charged Arg in the skeletal muscle channel decreased the fraction of slow-inactivated channels measured with a 10-s conditioning prepulse. Figure 4A shows that Na$_v$1.5 N406R channels were highly resistant to slow inactivation when tested with 50-s prepulses to a wide range of voltages. Despite the fact that only 20% of the current could be slow-inactivated, mibefradil affinity was affected less than 2-fold (4.8 versus 2.6 μM; Fig. 4B). While directionally consistent with the idea that slow inactivation controls mibefradil affinity, it did not rule out the possibility that this position might control affinity independent of its effects on slow inactivation.

To further probe for a relationship between slow inactivation and mibefradil affinity, we performed additional substitutions at position 406, substituting asparagine with uncharged or charged residues that varied in size and
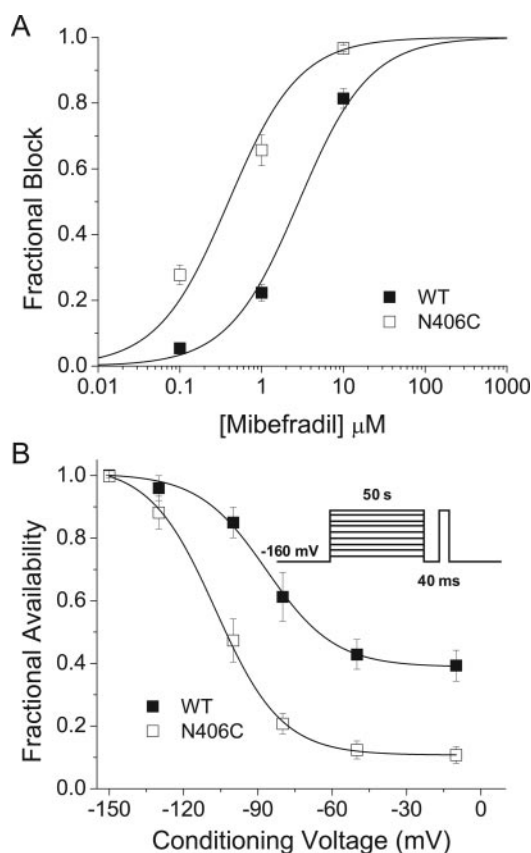
TABLE 1

Parameters for activation and inactivation kinetics of Na$_v$1.5 N405 channel mutants

The voltage half-points of activation and inactivation ($V_{1/2}$) and slope factors (dx) were derived from Boltzmann fits (as described in Figure 7). The uncharged substitutions (Ala, Cys, Phe) were made in the Na$_v$1.5 background (WT), whereas the charged substitutions (Asp, Glu, Arg, Lys) were performed in the Na$_v$1.5 C373Y (WT-C373Y) channel.

Channel	Activation		Inactivation	
	$V_{1/2}$ (n)	dx	$V_{1/2}$ (n)	dx
	mV			
WT	-47.6 ± 1.4 (19)	7.6 ± 0.5	-94.2 ± 1.5 (19)	5.4 ± 0.1
WT-C373Y	-46.7 ± 1.0 (9)	6.6 ± 0.1	-91.7 ± 1.5 (9)	5.3 ± 0.3
N406A	-24.8 ± 1.1 (19)	9.3 ± 0.2	-84.5 ± 1.0 (19)	5.7 ± 0.1
N406C	-44.1 ± 1.0 (13)	7.0 ± 0.3	-99.0 ± 1.0 (13)	6.0 ± 0.2
N406F	-31.8 ± 0.6 (12)	8.2 ± 0.2	-100.5 ± 1.3 (12)	5.7 ± 0.2
N406D	-35.2 ± 0.9 (16)	7.2 ± 0.1	-94.9 ± 1.3 (16)	4.9 ± 0.2
N406E	-55.4 ± 1.9 (8)	6.8 ± 0.3	-90.6 ± 2.2 (8)	5.5 ± 0.5
N406R	-46.8 ± 1.5 (9)	6.4 ± 0.2	-90.8 ± 1.9 (9)	4.9 ± 0.4
N406K	-48.2 ± 1.3 (16)	6.7 ± 0.1	-88.4 ± 1.5 (16)	4.1 ± 0.3

hydrophobicity, which, in the skeletal muscle isoform, exhibited varied effects on slow inactivation (Nau et al., 1999). Uncharged substitutions Ala and Phe enhanced slow inactivation (Fig. 5A) similar to N406C (Fig. 2, dashed line). If changes in mibefradil affinity were due to mutation-induced changes in slow inactivation, we would predict that replacing Asn406 with either Ala or Phe would increase affinity. Concentration-response curves shown in Fig. 5B, however, indicate this to be the case for only the N406F mutation, which exhibited a 4-fold lower IC_{50} for mibefradil block compared with WT (0.7 versus 2.9 μM). N406A, which also dramatically enhanced slow inactivation, however, had no effect on affinity. Furthermore, comparing across these uncharged substitutions, (Cys, Phe, and Ala), there was no obvious relationship between either the magnitude or voltage half-point of slow inactivation and mibefradil IC_{50} (Fig. 5, C and D), further suggesting that drug affinity and channel slow inactivation are being controlled independently of one another.

When Asn406 was substituted with the positively charged Arg, slow inactivation was almost abolished (Fig. 4). Substi-
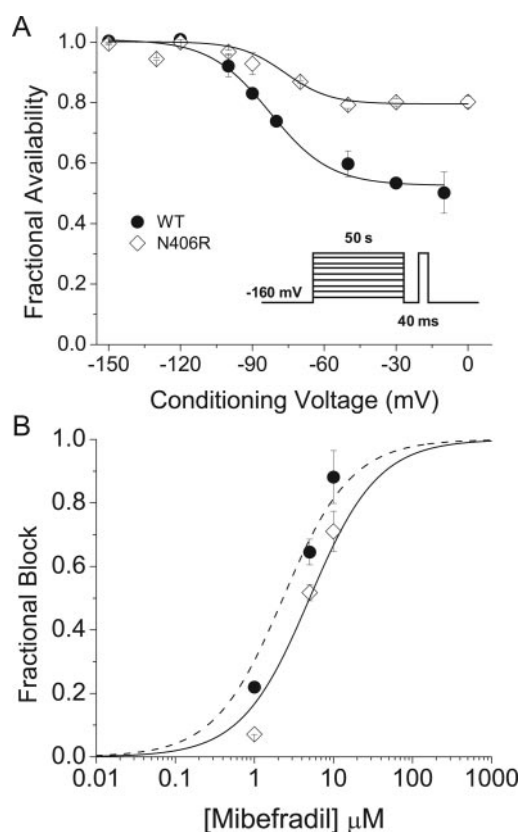
Fig. 3. Slow inactivation and mibefradil block of $Na_v1.5$ and $Na_v1.5$ C373Y. A, slow inactivation induced with 50 s inactivating prepulses in WT was compared with channels with a mutation (C373Y) in the outer pore, a maneuver that confers higher tetrodotoxin sensitivity to the cardiac isoform. Slow inactivation was measured using the same two-pulse protocol described in Fig. 2 and shown in the inset. Normalized averaged data (see Fig. 2 legend) recorded during the test pulse was plotted as a function of the conditioning prepulse and fit with a Boltzmann distribution to estimate parameters of slow inactivation which are shown in Table 2. $Na_v1.5$, $n = 3$; $Na_v1.5$ C373Y, $n = 5$. B, concentration-response data for mibefradil block of wild-type $Na_v1.5$ channels [taken from our previously published work (McNulty and Hanck, 2004)] and $Na_v1.5$ C373Y channels. Block was measured and IC_{50} was determined as described in Fig. 1. IC_{50}: WT, 2.9 32 ± 0.4 μM ($n = 5–6$ from McNulty and Hanck, 2004); C373Y, 2.6 ± 0.6 μM ($n = 2–3$ at each concentration)

TABLE 2

Parameters for slow inactivation kinetics of $Na_v1.5$ N405 channel mutants

Slow inactivation was measured as described in Figure 2. Data were fit with Boltzmann distribution to derive the voltage half-points of activation and inactivation ($V_{1/2}$) and slope factors (dx) and the steady state value of availability (S_2) (as described in Figure 2). The fraction of channels slow inactivated was determined from $1 - S_2$. The uncharged substitutions (Ala, Cys, Phe) were made in the $Na_v1.5$ background (WT), whereas the charged substitutions (Asp, Glu, Arg, Lys) were performed in the $Na_v1.5$ C373Y (WT-C373Y) channel. n values are given in the figure legends.

Channel	Slow Inactivation		Fraction	
	$V_{1/2}$	dx	Available S_2	Slow Inactivated $(1 - S_2)$
	mV			
WT	$-86.5 ± 5.6$	$13.8 ± 5.1$	$0.39 ± 0.05$	0.61
WT-C373Y	$-82.7 ± 0.01$	$12.6 ± 0.01$	$0.53 ± 0.001$	0.47
N406A	$-90.7 ± 0.2$	$4.7 ± 0.8$	$0.06 ± 0.01$	0.94
N406C	$-107.0 ± 4.1$	$13.3 ± 2.8$	$0.11 ± 0.02$	0.89
N406F	$-109.4 ± 7.6$	$6.1 ± 5.0$	$0.18 ± 0.01$	0.82
N406D	$-67.4 ± 6.7$	$13.4 ± 5.8$	$0.58 ± 0.04$	0.42
N406E	$-90.2 ± 2.0$	$3.7 ± 1.7$	$0.31 ± 0.02$	0.69
N406R	$-76.4 ± 1.5$	$9.4 ± 1.2$	$0.80 ± 0.01$	0.20
N406K	$-86.2 ± 3.9$	$3.1 ± 2.3$	$0.80 ± 0.02$	0.20

Fig. 4. Slow inactivation and mibefradil block of $Na_v1.5$ C373Y N406R channels. The N406R mutation was performed in the $Na_v1.5$ C373Y background. In this figure, WT refers to $Na_v1.5$ C373Y (data also shown in Fig. 3). A, slow inactivation was measured with the two pulse protocol described in Fig. 2 (inset). Normalized averaged data (see Fig. 2 legend) recorded during the test pulse were plotted as a function of the conditioning prepulse and fit with a Boltzmann distribution to estimate parameters of slow inactivation, which are shown in Table 2. Slow inactivation was reduced in N406R channels. WT C373Y, $n = 5$; C373Y N406R, $n = 2–4$ at each potential. B, concentration-response data for C373Y N406R channels. Mibefradil block was assayed as described for Fig. 1. Curves were fit with a single site binding curve to obtain IC_{50}: WT C373Y, $2.6 ± 0.6 \mu M$ ($n = 2$ or 3 at each concentration); C373Y N406R, $4.8 ± 0.2 \mu M$ ($n = 4$ or 5 at each concentration).

tution with Lys (K) also produced channels that slow-inactivated poorly (Fig. 6A). This effect was not limited to the introduction of a positively charged residue, in that the Asp substitution also inhibited slow inactivation, although for the slightly shorter Glu, slow inactivation was augmented. The variability in mutation-induced changes in slow inactivation allowed us to examine further whether a relationship exists between slow inactivation and mibefradil affinity. Figure 6, C and D, demonstrate that, similar to the uncharged substitutions, changes in mibefradil affinity did not correlate with alterations in either the voltage half-point ($V_{1/2}$) or the magnitude of slow inactivation, further supporting independence between the two processes.

Previous studies in brain and skeletal muscle Na$^+$ channel isoforms revealed important roles of this position in other kinetic parameters of channel gating, including those involved in activation and fast inactivation. As in the skeletal muscle Na$_v$1.4 channel, these substitutions in cardiac Na$_v$1.5 had widely different effects on activation gating. Two of the uncharged substitutions (Phe and Ala) shifted gating positively by approximately 16 and 23 mV, respectively (Fig. 7, Table 1), suggesting that these mutations destabilize the open state and/or stabilize the closed state. The cysteine and positively charged substitutions (Lys and Arg) had no effect on channel activation; whereas Glu hyperpolarized activation ~9 mV, whereas Asp shifted activation positively by ~12 mV. Effects of these substitutions on steady state inactivation, assayed with a 1-s conditioning prepulse (Fig. 7B; Table 1) were similarly diverse. For some, the shift in inactivation followed those observed in activation gating (Fig. 7C, Table 1); i.e., N406A shifted availability to the right by 10 mV.

Others, however (e.g., N406F, whose activation was also shifted positively), hyperpolarized steady-state availability (~6 mV), raising the possibility that this mutation alters coupling between activation and inactivation. Several other mutations had effects in one gating parameter but not the other. Therefore, it is clear that although substitutions at position 406 affect channel gating kinetics, changes in channel activation did not predict changes in channel availability and vice versa (Fig. 7C). Amino acid volume did not correlate with shifts in either activation or inactivation gating, indicating that amino acid size alone cannot explain the changes in voltage range over which these channels gate (data not shown). Many of these changes in channel gating are qualitatively consistent with alterations observed by Nau et al. (1999) in the skeletal channel, indicating that the effects of this position can be generalized across Na$^+$ channel isoforms.

Given the changes in channel gating kinetics apparent in conductance and channel availability, we more closely examined macroscopic current decay across mutations. Alterations in decay kinetics can significantly affect cellular excitability by regulating the magnitude of late Na$^+$ currents and potentially affect drug-channel interactions dependent on open channels. Visual inspection of currents between substitutions (Fig. 8A) indicated current time course was affected by substitutions at this position. The uncharged substitutions Cys and Ala had no statistically significant effect on decay kinetics (Fig. 8B, top); however, Phe sped decay kinetics across a wide voltage range (Fig. 8B, top inset). Furthermore, the charged substitutions, all of which elicited effects on activation, significantly slowed current decay (Fig. 8B, bottom). These data suggest that this position plays a
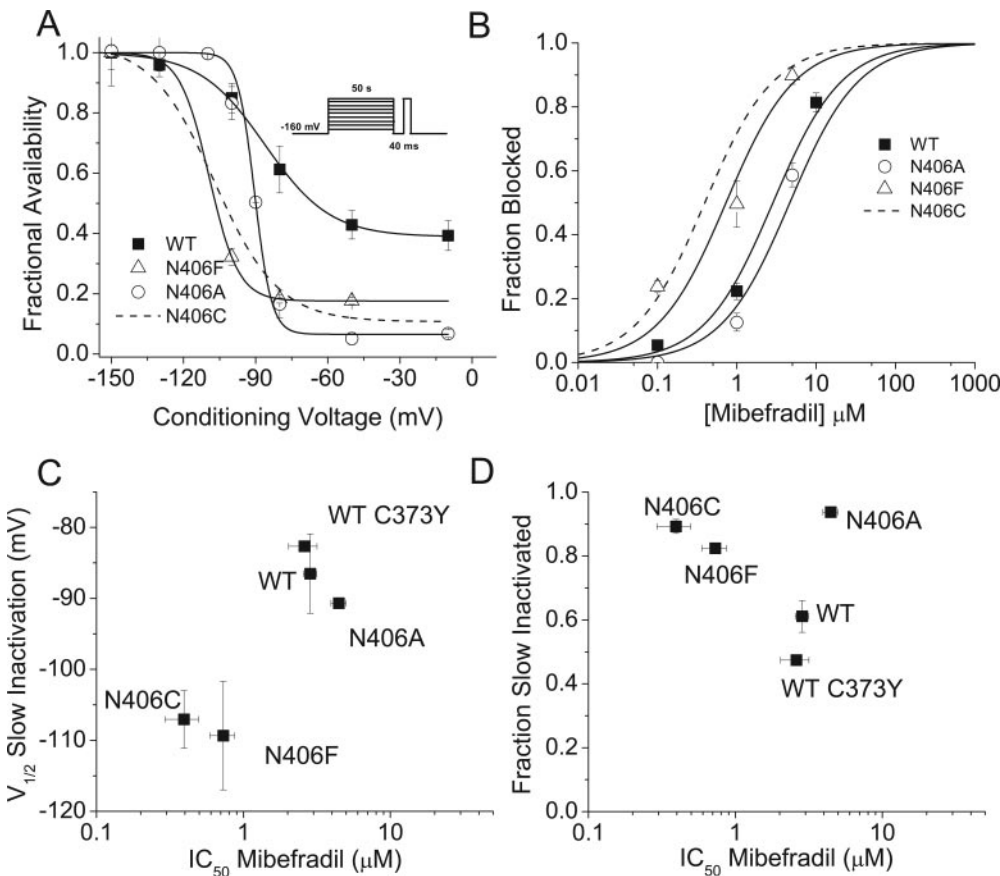

Fig. 5. Slow inactivation and mibefradil block of uncharged substitutions at Na$_v$1.5 Asn406. The dashed line depicts the N406C data shown in Fig. 2. Here, WT refers to Na$_v$1.5. A, slow inactivation was measured with the two-pulse protocol described in Fig. 2 and as shown in the inset. Normalized averaged data (see Fig. 2 legend) recorded during the test pulse was plotted as a function of the conditioning prepulse and fit with a Boltzmann distribution to estimate parameters of slow inactivation shown in Table 2. WT, $n = 3$; N406A, $n = 1$–5 at each potential; N406F, $n = 2$. B, concentration-response data for N406A and N406F channels. Mibefradil block was assayed as described for Fig. 1. Curves were fit with a single-site binding curve to obtain IC$_{50}$: WT, 2.9 ± 0.4 μM ($n = 5$–6 from McNulty and Hanck, 2004); N406A, 4.5 ± 0.5 μM ($n = 3$); N406F, 0.73 ± 0.14 ($n = 2$ or 3 at each concentration). C, the voltage half-points ($V_{1/2}$) derived from Boltzmann fits to the slow inactivation data for the uncharged mutations were plotted versus the IC$_{50}$ for mibefradil block. D, the steady-state values of availability derived from Boltzmann fits to slow inactivation data for the uncharged mutations were plotted as a function of the IC$_{50}$ for mibefradil block.

role in fast inactivation from the open state. It is noteworthy that although three of the substitutions (Asp, Arg, and Lys) exhibited decay kinetics closer to WT at more depolarized potentials (positive to −5 mV), the Glu mutation remained slower across the entire voltage range studied. Slowed decay could be the result of shifts in activation gating because decay kinetics speed with increasing depolarization. However, that was not the case with these mutations; substitutions that exhibited the slowest decay kinetics also exhibited the most negative voltage half-points of activation. There was also no inherent relationship between decay kinetics and channel availability or amino acid volume (data not shown).

Taken together, the data presented here demonstrate that an Asn in DI S6 (at position 406 in the cardiac $Na_v1.5$ channel) is an important regulator of channel gating across Na^+ channel isoforms. Furthermore, dramatic differences in mibefradil block across substitutions at 406, measured under conditions that should be unaffected by changes in channel gating, point to a location for Asn406 near or within the mibefradil binding site.

Discussion

The most straightforward explanation for the alterations in apparent affinity of mibefradil by mutations at Asn406 is that this position forms part of the mibefradil binding site, but before accepting this explanation, we evaluated whether substitutions exerted their effects on mibefradil block indirectly by altering channel gating, thus changing the proportion of channels in higher affinity conformations/states. Analysis of activation and inactivation and mibefradil affinity revealed no kinetic determinant. Our previous work demonstrated that mibefradil has a higher affinity for channels recruited to one or more slow-inactivated states (McNulty and Hanck, 2004), and the mutations that resulted in the channels with the most negative voltage range of slow inactivation (Cys, Phe) also exerted the most dramatic increase in mibefradil affinity, thus, of course, raising the question of whether a relationship exists between the propensity for these channels to slow inactivate and their sensitivity to mibefradil. However, other substitutions that either enhanced (Ala, Glu) or reduced (Lys, Arg, Asp) entry into slow-
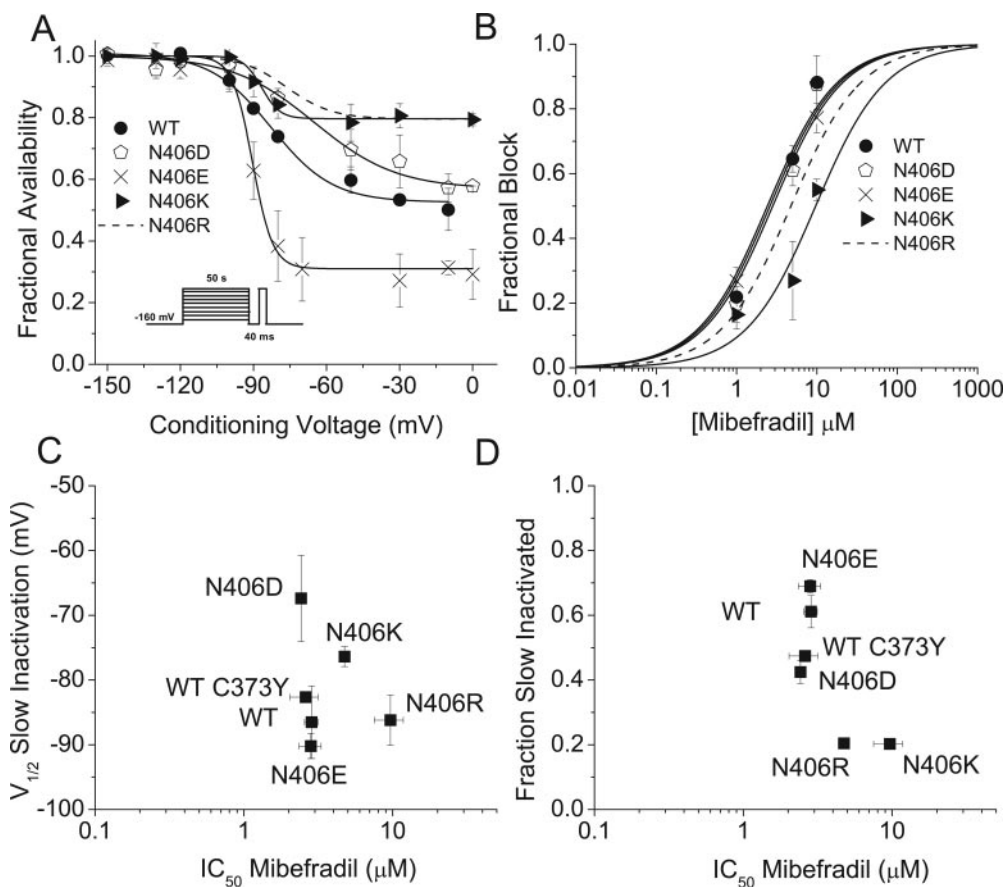

Fig. 6. Slow inactivation and mibefradil block of $Na_v1.5$ C373Y N406E, N406D, and N406K channels. Data for N406R (also shown in Fig. 4) are shown as a dashed line. All of the charged mutations were performed in the $Na_v1.5$ C373Y background. Here, WT refers to $Na_v1.5$ C373Y (data also shown in Fig. 3). A, slow inactivation was measured with the two pulse-protocol described in Fig. 2 and shown in the inset. Normalized averaged data (see Fig. 2 legend) recorded during the test pulse were plotted as a function of the conditioning prepulse and fit with a Boltzmann distribution to estimate parameters of slow inactivation shown in Table 2: WT C373Y, $n = 5$; C373Y N406E, $n = 3–7$ at each potential; C373Y N406D, $n = 1–5$ at each potential; C373Y N406K, $n = 3–9$ at each potential. B, concentration-response data for N406D, N406E, and N406K channels. Mibefradil block was assayed as described for Fig. 1. Curves were fit with a single site binding curve to obtain IC_{50}: WT C373Y, 2.6 ± 0.6 μM ($n = 2–3$ at each concentration); C373Y N406E, 2.8 ± 0.5 μM ($n = 4$ or 5 at each concentration); C373Y N406D, 2.4 ± 0.2 μM ($n = 3$); C373Y N406K, 9.7 ± 2.1 μM ($n = 4–7$ at each concentration). C, the voltage half-points ($V_{1/2}$) derived from Boltzmann fits to the slow inactivation data for the charged mutations were plotted versus the IC_{50} for mibefradil block. D, the steady-state values of availability derived from Boltzmann fits to slow inactivation data for the charged mutations were plotted as a function of the IC_{50} for mibefradil block.
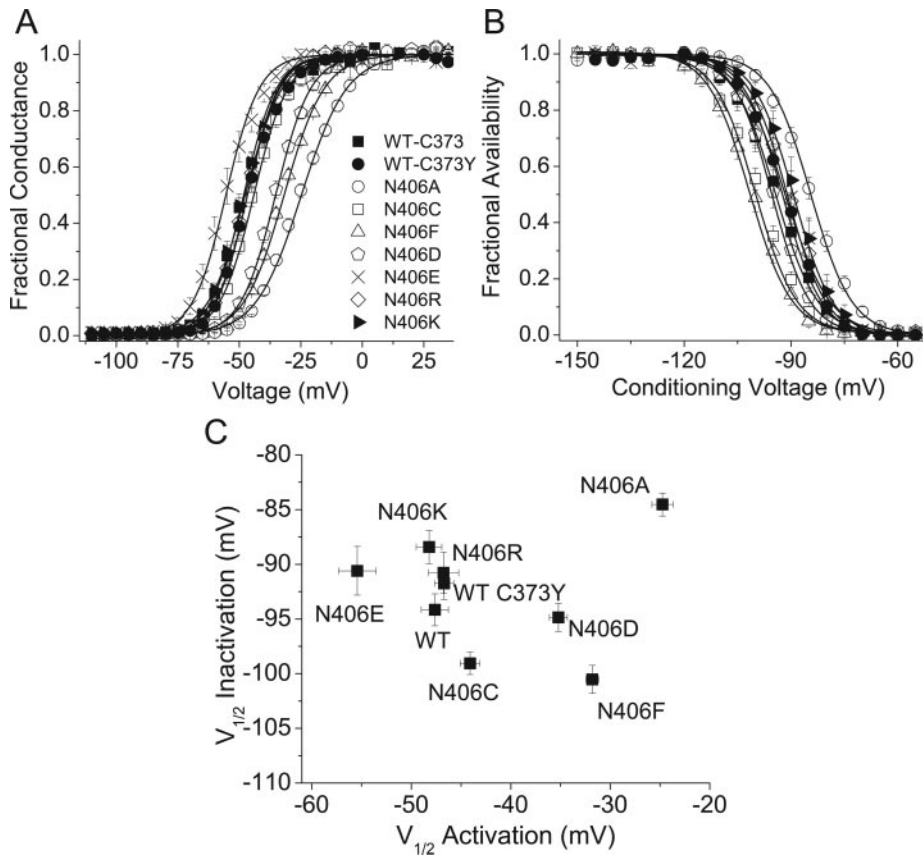
Fig. 7. Activation and fast inactivation for mutations at Asn406. The uncharged substitutions (Ala, Cys, Phe) were made in the Na$_v$1.5 background (WT), whereas the charged substitutions (Asp, Glu, Arg, Lys) were performed in the Na$_v$1.5 C373Y (WT-C373Y) channel. A, activation curves for all Asn406 mutations. Activation parameters were estimated by fitting current-voltage relationships with a transform of a Boltzmann distribution $I = (V - V_{rev}) \times G_{max}/(1 + \exp^{(V_{1/2} - V)/dx})$, where the peak Na$^+$ current (I) at each test voltage (V) was a function of the voltage for half-activation ($V_{1/2}$), dx is a slope factor, V_{rev} is the reversal potential, and G_{max} is maximal peak conductance. Estimated parameters derived from the Boltzmann fits are shown in Table 1. B, voltage-dependent channel availability was measured with a two-pulse protocol in which cells were first cells were depolarized for 1 s at potential ranging from -150 to -30 mV from a holding potential of -140, -150, or -160 mV before measuring Na$^+$ currents every 5 s at -30, -10, or 0 mV. Availability was fit with the following Boltzmann equation $I/I_{max} = 1/(1 + \exp^{(V - V_{1/2})/dx})$, where I is the peak current, I_{max} is the maximum peak current, V is the prepulse voltage, $V_{1/2}$ is the voltage for half-inactivation, and dx is the slope factor. Estimated parameters derived from the Boltzmann fits are shown in Table 1. C, the voltage half-points for activation are plotted against those for inactivation for mutations at Asn406.
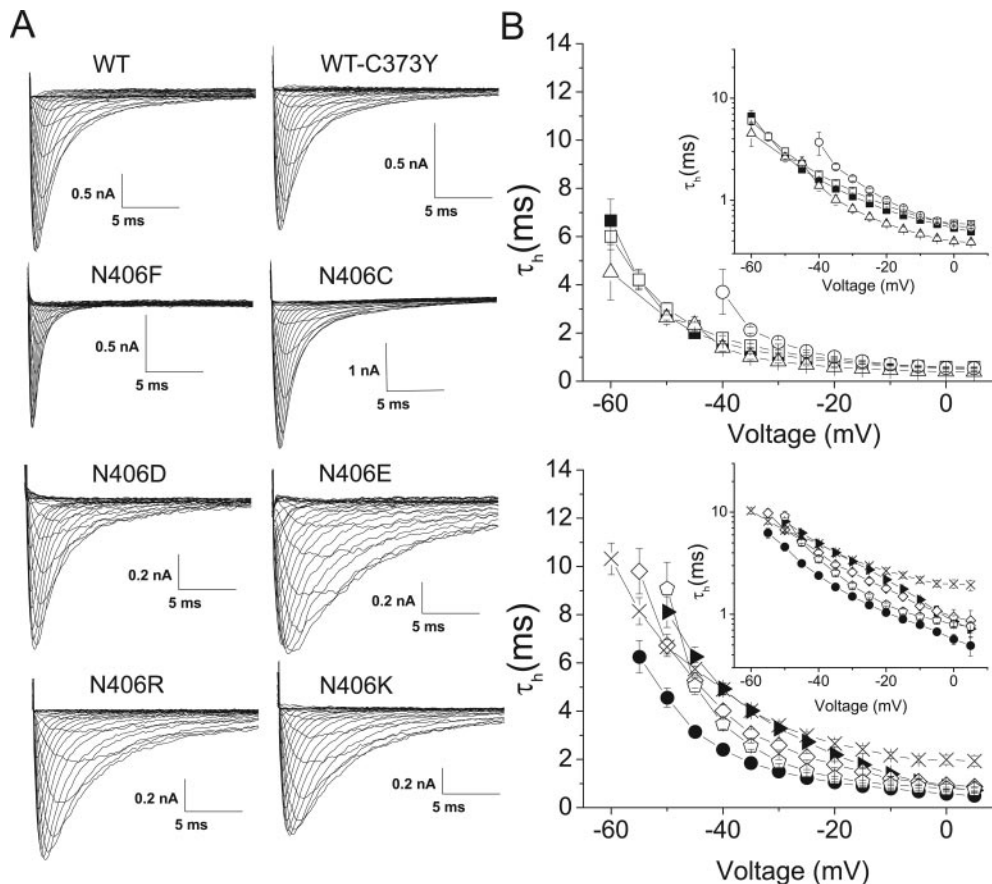

Fig. 8. Decay kinetics of charged mutations at Asn406. Uncharged substitutions were performed in the WT background, whereas the charged mutations were performed in WT-C373Y channels. A, representative current traces elicited with 20-ms depolarizations from a holding potential of -140 or -160 mV for WT, WT-C373Y, and mutations at position Asn406. Currents are noticeably slowed with the introduction of charge at Asn406 but faster with N406F. B, estimates for the time constants of current decay (τ_h) were derived by fitting current traces with the Hodgkin-Huxley m^{3}h formalism and plotted as a function of voltage. Top, τ_h values for the uncharged substitutions versus WT. ■, WT ($n = 19$); ○, N406A ($n = 19$); □, N406C ($n = 13$); △, N406F ($n = 12$). Across a wide voltage range, N406F has shorter decay time constants. Top, inset, the same data on a different scale to highlight the difference across mutants. $p < 0.05$ for N406F compared with WT. Bottom, τ_h values for the charged substitutions versus WT-C373Y. WT-● C373Y ($n = 9$); ⬠, N406D ($n = 16$); ×, N406E ($n = 8$); ◇, N406R ($n = 9$); and ▶, N406K ($n = 16$). Bottom, inset, the same data on a different scale to highlight the difference across mutants. Across a wide voltage range, N406R, N406K, and N406E channels exhibited longer time constants.

inactivated states had minimal effects on block. Furthermore, and perhaps more importantly, the voltage protocols used to assay mibefradil block strongly discouraged the accumulation of slow-inactivated states. Using short (20 ms) test steps and holding potentials far more negative than those over which slow inactivation occurred, our measurements should not have been affected by mutation-induced changes in slow inactivation.

Involvement of this position in slow inactivation gating has been studied most extensively in the skeletal muscle isoform. Wang and Wang (1997) were the first to demonstrate a dramatic enhancement of slow inactivation with an Ala substitution at Asn434 in $Na_v1.4$. Additional substitutions at this position in $Na_v1.4$ produced varied effects on the magnitude and voltage-dependence of slow inactivation (Nau et al., 1999; Kondratiev and Tomaselli, 2003) similar to alterations we observed here at Asn406 in $Na_v1.5$. The observations of Nau et al., (1999), for example, that Ala, Phe, and Cys substitutions at Asn434 in $Na_v1.4$ increased the magnitude of slow inactivation and hyperpolarized the voltage relationship of slow inactivation, are in rank order agreement with our data in $Na_v1.5$. Other substitutions at this position were also qualitatively similar across isoforms, reaffirming the generalizability of this Asn in slow inactivation gating. Quantitative differences between our data and those in the skeletal muscle isoform are probably the result of differences in the protocols used to assay slow inactivation and in the well documented differences in the magnitude and kinetics of slow inactivation between the cardiac and skeletal muscle channels (Richmond et al., 1998; O'Reilly et al., 1999).

The structural details underlying slow inactivation remain unclear but seem to involve rearrangements in both the inner and outer pores. We found here that a substitution of a residue in the outer pore (Cys373) from the cardiac-specific Cys to the skeletal muscle Tyr resulted in a channel more resistant to slow inactivation. O'Reilly and Shockett (2006) recently reported small differences in slow inactivation between these two channels that were directionally consistent with our data, although with their protocol, results did not reach statistical significance. In our experiments, slow inactivation was measured with conditioning prepulses that were 5 times longer (50 versus 10 s) than those used by O'Reilly and Shockett (2006), which could explain the quantitative differences between our data. The strong effects on slow inactivation exerted by substitutions at 406 and the location of this position within the inner pore may provide an additional clue into the structural basis of this process. However, it is important to note that a wide array of mutations scattered throughout the protein have also been shown to influence slow inactivation, and no pattern has yet emerged. In the meantime, however, we can use these channels as tools to examine interactions between channels and state-dependent drugs.

Substitutions at Asn406 in the cardiac $Na_v1.5$ channel did produce channels with kinetic differences, some quite dramatic, in both activation and inactivation gating, suggesting that Asn406 plays important roles in the conformational changes that occur during state transitions. The gating effects we observed in the cardiac $Na_v1.5$ channel were remarkably similar to those reported for other channel isoforms. Shifts in activation and fast inactivation gating induced by mutations at Asn406 in the cardiac channel were

qualitatively, and in many cases, quantitatively, consistent with the same mutations studied in either the $Na_v1.4$ background (at position Asn434) (Wang and Wang, 1997; Nau et al., 1999; Kondratiev and Tomaselli, 2003) or the $Na_v1.2$ channel (at position Asn418) (Yarov-Yarovoy et al., 2002). A comparative analysis of decay kinetics across mutations was not reported in the previous studies; however, Wang and Wang (1997) found that the Ala substitution at Asn434 in $Na_v1.4$ sped kinetics at potentials positive to +20 mV. We observed no change in decay kinetics with the N406A mutation, a result that could reflect differences in the voltage range examined or gating properties between isoforms. Wang et al. (1998), however, did note persistent late currents with the Asp mutation in $Na_v1.4$, consistent with our observation
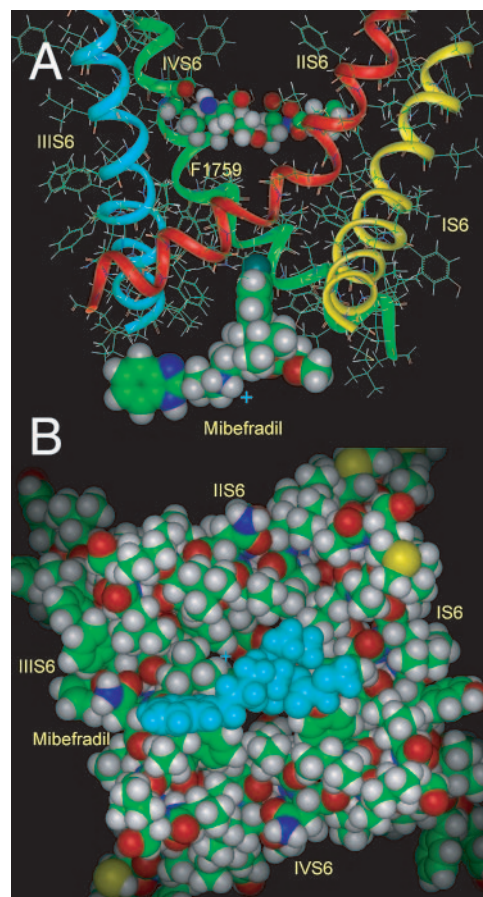

Fig. 9. A proposed model for the binding of mibefradil in the open pore of $Na_v1.5$. Channel coordinates are those from Lipkind and Fozzard (2005), and crystal coordinates for mibefradil were kindly provided by Roche Pharmaceuticals. A, side view of S6 helices as ribbons (yellow, red, cyan, and green) with selectivity filter residues (DEKA) shown by balls and sticks. The domain IV S6 residue found to be most important for binding local anesthetics (Phe1759) is noted. Mibefradil, shown space-filled, was oriented so as to make direct van der Waals contacts between the rigid benzene cyclohexene moiety of mibefradil and the aromatic ring of Phe in the N406F mutant channel. In this placement, the amine of mibefradil is oriented toward the cytoplasm, and the benzene cyclohexene moiety extends only a small distance into the pore, not making contacts with residues previously shown to affect binding of local anesthetics (Fig. 1). The selectivity filter is greater than 18 Å above the long axis of mibefradil. B, view of the drug in the channel as seen from the intracellular side. S6 helices are shown space-filled, and mibefradil is now cyan. Note that mibefradil (14 × 21 Å) lies across the open pore entrance (15 Å at this level), acting as a plug. This orientation not only occludes the pore and inhibits permeation but also is consistent with the binding data of Eller et al. (2000), who demonstrated that mibefradil analogs with widely different lengths of amine substituents produced similar affinities.

that introduction of charge at 406 slowed decay kinetics across a defined voltage range, suggesting a role of this position in fast inactivation from the open state. The fact that a similar pattern of gating effects emerges across multiple isoforms suggests that this Asn in DI S6 plays important "global" roles in conformational changes underlying transitions across channel states that are isoform-independent.

We are far from having a complete picture of mibefradil's state-dependent binding properties. However, we can use a homology model of the open Na$^+$ channel pore to propose general docking that is consistent with the data presented here, as well as the available data from the literature. Lipkind and Fozzard (2005) recently created a model of an open Na$^+$ channel pore that allowed for the docking of pore-blocking LA drugs. Their model, which used information from the crystal structure of the bacterial MthK K$^+$ channel in the open conformation (Jiang et al., 2002), proposed an inner pore of ~18 Å in length (from the selectivity filter to the cytoplasm) that measures ~6 Å across (just beneath the selectivity filter) and expands to a width of 15 Å at the level of the Asn. Available mutagenesis data indicate that LA compounds dock deep in the inner pore just under the selectivity filter in this model (Fig. 9; Phe1759, the most important binding determinant is labeled). On the other hand, we found that inner pore residues critical for LA block did not affect mibefradil block, suggesting that its affinity is controlled at a distinct site. As a large, bulky, and rigid molecule (measuring 14 Å in length by 21 Å across), steric hindrances probably prevent mibefradil from binding deep within the inner pore. The N406F mutation produced a 4-fold improvement in affinity, suggesting that this channel can make a more favorable interaction with mibefradil. Indeed, if mibefradil is docked so as to allow the benzene cyclohexene moiety to make an aromatic-aromatic interaction with the Phe, the long rigid mibefradil molecule rests across the inner mouth of the channel, with the benzene cyclohexene moiety extending only partially into the inner mouth. Such a position is a particularly attractive proposal, since Eller et al. (2000) found that increasing the volume and length of mibefradil by adding long-chain and/or aromatic substituents on the methylaminoethyl nitrogen [thus replacing the 3-(2-benzimidazoyl) propyl group or extending its distance from the nitrogen] did not alter binding affinity, suggesting that mibefradil does not fit deep within the inner pore to block current. Such a position would also be consistent with the finding that mibefradil and phenylalkylamines compete (Rutledge and Triggle, 1995), because, even though they would not be predicted to share a formal binding site, mibefradil occupancy would preclude phenylalkylamines from reaching their binding site located within the inner pore. Data are not yet available for the analogous mutation in Ca^{2+} channels; however, as a residue that is highly conserved across multiple isoforms of both Na$^+$ and Ca^{2+} channels, the Asn at this position represents an attractive candidate drug binding determinant that may form the basis of mibefradil's cross-reactivity. Overall, these data and the proposed binding presented here support the idea that mibefradil block is controlled by a region of the channel near the inner pore that includes or is near the Asn at 406, a residue that also plays important roles in channel gating across Na$^+$ channel isoforms.

References

Catterall WA (2000) Structure and regulation of voltage-gated Ca^{2+} channels. *Annu Rev Cell Dev Biol* **16:**521–555.
Catterall WA (2002) Molecular mechanisms of gating and drug block of sodium channels. *Novartis Found Symp* **241:**206–218; discussion 218–232.
Chouabe C, Drici MD, Romey G, Barhanin J, and Lazdunski M (1998) HERG and KvLQT1/IsK, the cardiac K$^+$ channels involved in long QT syndromes, are targets for calcium channel blockers. *Mol Pharmacol* **54:**695–703.
Eller P, Berjukov S, Wanner S, Huber I, Hering S, Knaus HG, Toth G, Kimball SD, and Striessnig J (2000) High affinity interaction of mibefradil with voltage-gated calcium and sodium channels. *Br J Pharmacol* **130:**669–677.
Fozzard HA and Hanck DA (1996) Structure and function of voltage-dependent sodium channels: comparison of brain II and cardiac isoforms. *Physiol Rev* **76:**887–926.
Guatimosim S, Sobie EA, dos Santos Cruz J, Martin LA, and Lederer WJ (2001) Molecular identification of a TTX-sensitive Ca^{2+} current. *Am J Physiol* **280:**C1327–C1339.
Hartmann HA, Tiedeman AA, Chen SF, Brown AM, and Kirsch GE (1994) Effects of III-IV linker mutations on human heart Na$^+$ channel inactivation gating. *Circ Res* **75:**114–122.
Jiang Y, Lee A, Chen J, Cadene M, Chait BT, and MacKinnon R (2002) Crystal structure and mechanism of a calcium-gated potassium channel. *Nature (Lond)* **417:**515–522.
Kondratiev A and Tomaselli GF (2003) Altered gating and local anesthetic block mediated by residues in the I-S6 and II-S6 transmembrane segments of voltage-dependent Na$^+$ channels. *Mol Pharmacol* **64:**741–752.
Lipkind GM and Fozzard HA (2005) Molecular modeling of local anesthetic drug binding by voltage-gated sodium channels. *Mol Pharmacol* **68:**1611–1622.
Martin RL, Lee JH, Cribbs LL, Perez-Reyes E, and Hanck DA (2000) Mibefradil block of cloned T-type calcium channels. *J Pharmacol Exp Ther* **295:**302–308.
McNulty MM and Hanck DA (2004) State-dependent mibefradil block of Na$^+$ channels. *Mol Pharmacol* **66:**1652–1661.
Nau C, Wang SY, Strichartz GR, and Wang GK (1999) Point mutations at N434 in D1–S6 of μ1 Na(+) channels modulate binding affinity and stereoselectivity of local anesthetic enantiomers. *Mol Pharmacol* **56:**404–413.
Nilius B, Prenen J, Kamouchi M, Viana F, Voets T, and Droogmans G (1997) Inhibition by mibefradil, a novel calcium channel antagonist, of Ca^{2+}- and volume-activated Cl$^-$ channels in macrovascular endothelial cells. *Br J Pharmacol* **121:**547–555.
O'Reilly JP and Shockett PE (2006) Slow-inactivation induced conformational change in domain 2-segment 6 of cardiac Na$^+$ channel. *Biochem Biophys Res Commun.*
O'Reilly JP, Wang SY, Kallen RG, and Wang GK (1999) Comparison of slow inactivation in human heart and rat skeletal muscle Na$^+$ channel chimaeras. *J Physiol* **515:**61–73.
Perchenet L and Clement-Chomienne O (2000) Characterization of mibefradil block of the human heart delayed rectifier hKv1.5. *J Pharmacol Exp Ther* **295:**771–778.
Richmond JE, Featherstone DE, Hartmann HA, and Ruben PC (1998) Slow inactivation in human cardiac sodium channels. *Biophys J* **74:**2945–2952.
Rutledge A and Triggle DJ (1995) The binding interactions of Ro 40-5967 at the L-type Ca^{2+} channel in cardiac tissue. *Eur J Pharmacol* **280:**155–158.
Satin J, Kyle JW, Chen M, Bell P, Cribbs LL, Fozzard HA, and Rogart RB (1992) A mutant of TTX-resistant cardiac sodium channels with TTX-sensitive properties. *Science (Wash DC)* **256:**1202–1205.
Townsend C and Horn R (1997) Effect of alkali metal cations on slow inactivation of cardiac Na$^+$ channels. *J Gen Physiol* **110:**23–33.
Wang GK, Quan C, and Wang SY (1998) Local anesthetic block of batrachotoxin-resistant muscle Na$^+$ channels. *Mol Pharmacol* **54:**389–396.
Wang SY and Wang GK (1997) A mutation in segment I-S6 alters slow inactivation of sodium channels. *Biophys J* **72:**1633–1640.
Wang SY and Wang GK (1998) Point mutations in segment I-S6 render voltage-gated Na$^+$ channels resistant to batrachotoxin. *Proc Natl Acad Sci USA* **95:**2653–2658.
Yarov-Yarovoy V, McPhee JC, Idsvoog D, Pate C, Scheuer T, and Catterall WA (2002) Role of amino acid residues in transmembrane segments IS6 and IIS6 of the Na$^+$ channel alpha subunit in voltage-dependent gating and drug block. *J Biol Chem* **277:**35393–35401.

Address correspondence to: Dorothy A. Hanck, 5841 S. Maryland Ave, MC6094, Chicago, IL 60637. E-mail: dhanck@uchicago.edu